Investigation of MHD fractionalized viscous fluid and thermal memory with slip and Newtonian heating effect: a fractional model based on Mittag-Leffler kernel

Qasim Ali[1] · Muhammad Amir[2] · Ahmed Sayed M. Metwally[3] · Usman Younas[4] · Ahmed Zubair Jan[5] · Ayesha Amjad[6]

Abstract

This paper introduces an innovative approach for modelling unsteady incompressible natural convection flow over an inclined oscillating plate with an inclined magnetic effect that employs the Atangana-Baleanu time-fractional derivative (having a non-singular and non-local kernel) and the Mittag-Leffler function. The fractional model, which includes Fourier and Fick's equations, investigates memory effects and is solved using the Laplace transform. The Mittag-Leffler function captures power-law relaxation dynamics, which improves our understanding of thermal and fluid behaviour. Graphical examination shows the influence of fractional and physically involved parameters, leading to the conclusion that concentration, temperature, and velocity profiles initially grow and then decrease asymptotically with time. Moreover, the study emphasizes the impact of effective Prandtl and Schmidt numbers on temperature, concentration, and velocity levels in the fluid.

Abbreviations

AB	Atangana-Balenau-time-fractional derivative
NF	Nanofluids
HNF	Hybrid-nanofluid
MHD	Magnetohydrodynamics
PDEs	Partial differential equations

List of symbols

w	Fluid velocity $\left(\mathrm{m\,s^{-1}}\right)$
t	Times (s)
g	Gravity acceleration $\left(\mathrm{m\,s^{-2}}\right)$
K	Thermal conductivity of the fluid $\left(\mathrm{W\,m^{-1}\,k^{-1}}\right)$
C_f	Skin friction
ρ	Fluid density $\left(\mathrm{kgm^{-3}}\right)$
U_0	Characteristic velocity $\left(\mathrm{ms^{-1}}\right)$
θ_1	The angle of magnetic inclination
θ_2	The inclination angle of the plate
ψ	Concentration of fluid $\left(\mathrm{mol\,m^{-3}}\right)$
$\mathrm{Pr_{eff}}$	Effective Prandtl number
ϕ	Temperature of the fluid (K)
B_o	Strength of magnetic field $\left(\mathrm{Kg\,s^{-2}}\right)$
M	Magnetic parameter (K)
Re	Reynold's number
Sc	Schmidt number

✉ Ahmed Zubair Jan
ahmed.jan@pwr.edu.pl

Qasim Ali
aliqasim829@gmail.com

Muhammad Amir
amirramzan423@gmail.com

Ahmed Sayed M. Metwally
dalsayed@ksu.edu.sa

Usman Younas
usmanalgebra@yahoo.com

Ayesha Amjad
Ayesha.amjad@polsl.pl

1   Department of Mathematics, University of Chakwal, Chakwal 48800, Pakistan

2   Department of Mathematics, University of Engineering and Technology, Lahore 54890, Pakistan

3   Department of Mathematics, College of Science, King Saud University, 11451 Riyadh, Saudi Arabia

4   Department of Mathematics, Shanghai University, Shanghai, China

5   Department of Mechanical Engineering, Wroclaw University of Science and Technology, Wroclaw, Poland

6   Faculty of Transport and Aviation Engineering, Silesian University of Technology, Krasińskiego 8 Street, 40-019 Katowice, Poland

q	Laplace transform variable
β_ϕ	Volumetric coefficient of thermal expansion $\left(\mathrm{k}^{-1}\right)$
ϕ_∞	Ambient temperature (K)
Gr	Grashof number
ν	Kinematic viscosity $\left(\mathrm{m}^2\,\mathrm{s}^{-1}\right)$
Gm	Mass Grashof number
C_p	Specific heat at constant pressure $\left(\mathrm{J\,kg^{-1}K^{-1}}\right)$
Sh	Sherwood number
γ	Fractional parameter
Nu	Nusselt number
σ	Electrical conductivity
H	Slip parameter

Introduction

Natural convection flows phenomena happen broadly in nature and are generally significant in solar energy collectors, purification processes, atmospheric, refrigeration of nuclear reactors, and oceanic circulation that occur in fluid mechanics if the temperature does vary density differences, leading to buoyant effects that affect its motion. Insights on utilizing natural convective flows may be seen in [1–4]

Akram et al. [6] investigated the impacts of MHD NF flow on peristaltic waves along with viscous dissipation as well as convection produced by slip effects through a channel, by employing the extensive wavelength and little but finite Reynold number estimation process. Sadia et al. [7] discussed a second-grade fluid motion produced by employing a permeable disc taking partial slip character. Thermal transmission made by heating the disc surface as well as by ohmic and viscous heating effects are evaluated and modelled with a thermal slip state. Associated mass transmission phenomena with thermophoretic distribution are also articulated. Further, the implementation of velocity slip supposition encourages non-linearity in the boundary situations in velocity mechanisms. Abidin et al. [8] studied a Carreau NF flow in a channel by Bvp4c technique of MATLAB. The concentration as well as energy equations is supposed by employing conservation and Navier–Stokes equations utilizing the revised Buongiorno model. They proved that temperature distribution rises along with heat source, thermal radiation, nanoscale effects, and Brinkman number. The fractional Oldroyd-B HNF with important impacts like wall slip condition, constant concentration, and Newtonian heating which further categorizes the behaviour of HNF flow and thermal transmission phenomena in a good manner was examined by the Laplace method. They also studied fractionalized Oldroyd-B HNF and second-grade NF based on AB and Prabhakar fractional techniques [9, 10]. A fractionalized MHD as well as the thermal transfer of a Brinkman tri-HNF in a porous medium with ramped conditions and generalized velocity in a vertical plate was discussed by utilizing AB differentiation and the Laplace approach.

Further, a convection flow of a fractional HNF in a microchannel containing two parallel plates separately was considered with Newtonian heating impacts with the Caputo–Fabrizio (CF) and Laplace's approach by Amir et al. [11, 12].

The effects of Newtonian heating constraint with free convection fluid flowing were examined by Vieru et al. [13]. The problems for an incompressible flow with chemical reactions for some different fluids over a plate were considered in [14]. Viscous dissoluteness as well as the effect of the Joule heating scheme is investigated in [15]. The Newtonian heating impacts for the three-dimensional MHD flow with a special form of pressure were studied in [16]. A particular form of movement with Newtonian heating effect and power-law NF was discussed by Hayat et al. [17].

Free convective MHD flow with slip condition was investigated in [18]. They considered the Newtonian heating impacts with a nonlinear elastic plate in their research. Kamran et al. [19] discoursed Newtonian heating with the convective flow by using chemical reactions and boundary slip conditions. The characteristics of Newtonian heating were deliberated in [20] because of the motion of a micropolar fluid with a flexible plate. The spectral relaxation technique was used to discuss the NF for MHD flow through a channel flow in [21]. The consequences of Newtonian heating, heat generation, and organic response were studied [22] by considering Casson fluid flow on a moving plate placed with a permeable media. The flow of non-Newtonian fluid by taking into mind the viscosity and Newtonian heating effect was examined by Ahmad et al. [23].

The perception of fractional order and integral operators has suggestively affected several areas of applied sciences, engineering, and technology. In 1967, the perception of fractional calculus was developed from Caputo's research work [24] in the year of 1967 and projected a characterization of the fractional derivative. This description helps use the integral transform method with an initial condition.

Moreover, this method was useful to find the solution to numerous physical mathematical problems. However, Caputo and Fabrizio studied that this non-integer technique has few drawbacks that yield indeterminate outcomes mostly for the structure and explanation of applied models. Hereafter, some well-known investigators appealed that such ambiguous consequences are due to singularity in the complicated integral. Their suggestion was useful and attentive. Subsequently, Caputo and Fabrizio proposed an innovative fractional derivative lacking a singularity [25].

Numerous researchers efficiently applied the Caputo-Fabrizio operator method in their work [26]. After this, a novel fractional order derivative also acknowledged oppositions due to the non-local kernel. So, Atangana and Baleanu presented an innovative non-integer operator involving a non-singular as well as non-local kernel [27]. Newly, many

researchers are applying these non-integer operators having the Mittag-Leffler function. However, a more systematic and comprehensive investigation of these recent techniques is still compulsory. Lin et al. [28] used the Laplace technique to study a Casson fluid fractional model that included two parallel plates subjected to magnetic force. El-Zahar et al. [29] solved a fractionalized convection–diffusion system with a modified residual power series approach. Demir et al. [30] investigated a proportional Caputo-hybrid technique with a novel feature for this operator. Furthermore, they demonstrated how results build on and improve on prior findings in the system of integral inequalities. Chu et al. [31] examined a fractional third-order dispersive system using a variational iteration transform approach and the Shehu decomposition method. Raza et al. [32] used a nonlinear fractional system with the AB derivative to define COVID-19. They used the Toufik-Atangana approach to provide numerical solutions for the fractional model. Majeed et al. studied Newtonian and non-Newtonian fluids with different circumstances i.e. viscous fluid flow between two discs, with a hexagonal cavity, Maxwell fluid flow with Keller box-scheme, flow and thermal transfer over a pair of heated bluff bodies through a channel and presented important results in the literature [33–35]. Different researchers discussed flow in a channel; in a wavy trapezoidal cavity, MHD flows with slip conditions and periodic flow in no-Newtonian fluid [37–39].

The study of MHD fractionalized viscous fluids with thermal memory, slip, and Newtonian heating effects is very important in many scientific and engineering disciplines. Understanding these complex fluid dynamics is critical for optimizing heat transfer operations in industrial systems, increasing the performance of energy conversion devices, and designing innovative cooling systems. Further, the proposed fractional model, which employs the Atangana-Baleanu time-fractional approach and the Mittag-Leffler kernel, advances mathematical modelling methods to describe phenomena involving non-local and memory-dependent effects, providing a valuable tool for investigators in fluid dynamics as well as applied mathematics. This study's findings are poised to manipulate diverse fields, including materials science and environmental engineering, by giving insights into the complicated interplay of magnetic fields, thermal memory, and fractional calculus in fluid systems [41–45].

In the above literature, we see that the investigation of the Newtonian heating influence in numerous sceneries is a substantial practical as well as theoretical study for the solution of significant problems based on the non-integer derivative. After receiving inspiration from these facts, our main goal is to examine the influences of Newtonian heating on incompressible natural convection unsteady and viscous flow over an oscillating infinite inclined plate with an inclined magnetic field by employing fractional operator with Mittag-Leffler memory. The Laplace transform is invoked for the numerical

and fractional simulations. To accomplish the Laplace inversion, two different approaches, Tzou technique and Stehfest are used. Finally, a graphical investigation of fractional and flow parameters is done by employing MathCad15 and discussed.

Problem statement based on Atangana-Balenau-time-fractional derivative

We consider unsteady and free convection viscous flow over an oscillating inclined plate with an inclined magnetic field having a strength B_o. Initially, fluid and the inclined plate having an ambient medium temperature ϕ_∞ and concentration value of ψ_∞. At $t > 0^+$, the fixed plate starts oscillating through velocity $U_o\cos(\omega t)$. The values of thermal as well as concentration also increase over time as revealed in Fig. 1. With the above conditions and using Boussinseq's estimation, the governing equations for this problem are [5]

$$
\begin{aligned}
\frac{\partial w(y,t)}{\partial t} &= v\frac{\partial^2 w(y,t)}{\partial y^2} - \frac{\sigma B_o^2}{\rho}\sin(\theta_1)w(y,t) \\
&+ g\beta_\phi\big(\phi(y,t) - \phi_\infty\big)\cos(\theta_2) \\
&+ g\beta_\psi\big(\psi(y,t) - \psi_\infty\big)\cos(\theta_2).
\end{aligned}
\tag{1}
$$

$$
\rho C_p\frac{\partial \phi(y,t)}{\partial t} = -\frac{\partial \xi(y,t)}{\partial y}.
\tag{2}
$$

$$
\xi(y,t) = -K\frac{\partial \phi(y,t)}{\partial y}.
\tag{3}
$$

$$
\frac{\partial \psi(y,t)}{\partial t} = -\frac{\partial \eta(y,t)}{\partial y} - K\big(\psi(y,t) - \psi_\infty\big).
\tag{4}
$$

$$
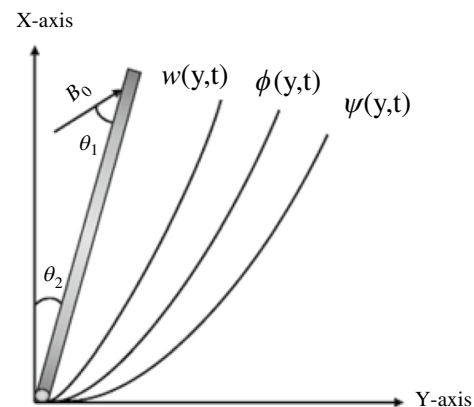\eta(y,t) = -D\frac{\partial \psi(y,t)}{\partial y}.
\tag{5}
$$

Fig. 1 Flow geometry

where $\xi(y, t), \eta(y, t)$ indicates the thermal and mass fluxes by Fourier as well as Fick's law.

The following are the supposed physical initial boundary conditions

$$w(y, 0) = 0, \phi(y, 0) = \phi_\infty, \psi(y, 0) = \psi_\infty; \ y \geq 0 \qquad (6)$$

$$w(0, t) - h \frac{\partial w(y, t)}{\partial y}\bigg|_{y=0} = U_o \cos(\omega t), \ \frac{\partial \phi(y, t)}{\partial y}\bigg|_{y=0}$$
$$= -\frac{h}{k} \phi(0, t), \ \psi(0, t) = \psi_w; \ t > 0 \qquad (7)$$

$$w(y, t) \to 0, \quad \phi(y, t) \to \phi_\infty, \quad \psi(y, t) \to \psi_\infty \text{ as } y \to \infty \qquad (8)$$

By introducing the following dimensionless parameters and functional values

$$w^* = \frac{K}{\nu h} w, \ y^* = \frac{h}{K} y, \ t^* = \frac{Kg}{h\nu} t, \ \phi^* = \frac{\phi(y, t) - \phi_\infty}{\phi_w - \phi_\infty},$$
$$\text{Re} = \left(\frac{h}{K}\right)^3 \frac{\nu^2}{g}$$

$$\psi^* = \frac{w(y, t) - \psi_\infty}{\psi_w - \psi_\infty}, \ k^* = k\frac{\nu}{g}\left(\frac{h}{K}\right), \ \xi^* = \frac{\xi}{\xi_o}, \ \eta^* = \frac{\eta}{\eta_o}.$$

Into Eqs. (1–8) and ignore the steric notation. We have

$$\frac{\partial w(y, t)}{\partial t} = \text{Re} \frac{\partial^2 w(y, t)}{\partial y^2} - M \sin(\theta_1) w(y, t)$$
$$+ \text{GrCos}(\theta_2) \phi(y, t) + \text{GmCos}(\theta_2) \psi(y, t). \qquad (9)$$

$$\Pr_{\text{eff}} \frac{\partial \phi}{\partial t} = -\frac{\partial \xi}{\partial y}. \qquad (10)$$

$$\xi(y, t) = -k \frac{\partial \phi}{\partial y}. \qquad (11)$$

$$\text{Sc}_{\text{eff}} \frac{\partial \psi(y, t)}{\partial t} = -\frac{\partial \eta(y, t)}{\partial y} - k\text{Sc}_{\text{eff}} \psi(y, t). \qquad (12)$$

$$\eta(y, t) = -\frac{\partial \psi(y, t)}{\partial y}. \qquad (13)$$

$$w(y, 0) = 0, \phi(y, 0) = 0, \psi(y, 0) = 0; \ y \geq 0, \qquad (14)$$

$$w(0, t) - h \frac{\partial w(y, t)}{\partial y}\bigg|_{y=0} = \cos(\omega t), \ \frac{\partial \phi(y, t)}{\partial y}\bigg|_{y=0}$$
$$= -(1 + \phi(0, t)), \ \psi(0, t) = 1, \qquad (15)$$

$$w(y, t) \to 0, \quad \phi(y, t) \to 0, \quad \psi(y, t) \to 0 \text{ as } y \to \infty. \qquad (16)$$

where

$$\Pr = \frac{\mu C_p}{K}, \text{Gr} = \frac{g(\nu\beta_\phi)_f(\phi_w - \phi_\infty)}{\nu_o^2}, \ \text{Sc} = \frac{\nu}{D}, \ \Pr_{\text{eff}} = \frac{\Pr}{\text{Re}}, \ \text{Sc}_{\text{eff}} = \frac{\text{Sc}}{\text{Re}}.$$

Formulation of fractional model by using AB fractional derivative

To construct a fractional model recently introduced fractional derivative i.e. AB derivative is utilized, which is stated as [32, 33] for the function $\eta(\xi, t)$.

$$^{AB}\mathfrak{D}_t^\gamma \eta(\xi, t) = \frac{1}{1 - \gamma} \int_0^t E_\gamma \left[\frac{\gamma(t - z)^\gamma}{1 - \gamma} \right] \eta'(\xi, t) dt; \ 0 < \gamma < 1 \qquad (17)$$

and $E_\gamma(z)$ is a Mittage-Lefflerr function demarcated as

$$E_\gamma(z) = \sum_{i=0}^\infty \frac{z^\gamma}{\Gamma(i\gamma + 1)}; \ 0 < \gamma < 1, z \in \mathbb{C}. \qquad (18)$$

$$\mathcal{L}\left\{ ^{AB}\mathfrak{D}_t^\gamma \eta(\xi, t) \right\} = \frac{q^\gamma \mathcal{L}[\eta(\xi, t)] - q^{\gamma-1} \eta(\xi, 0)}{(1 - \eta)q^\gamma + \gamma}, \qquad (19)$$

with

$$\lim_{\gamma \to 1} {}^{AB}\mathfrak{D}_t^\gamma \eta(\xi, t) = \frac{\partial \eta(\xi, t)}{\partial t}. \qquad (20)$$

In this investigation, we have used an effective fractional approach i.e. AB time-fractional operator to investigate the thermal memory in view of generalized Fourier and Fick's law [32, 33]

$$\xi(y, t) = -{}^{AB}\mathfrak{D}_t^\gamma \frac{\partial \phi(y, t)}{\partial y}. \qquad (21)$$

$$\eta(y, t) = -{}^{AB}\mathfrak{D}_t^\gamma \frac{\partial \psi(y, t)}{\partial y}. \qquad (22)$$

Solution of the problem

Temperature field

Applying the Laplace transform on Eqs. (10 and 21) and conditions $(14)_2$–$(16)_2$, we get

$$\Pr_{\text{eff}} q\bar{\phi}(y, q) = \frac{q^\gamma}{(1 - \gamma)q^\gamma + \gamma} \frac{\partial^2 \bar{\phi}(y, q)}{\partial y^2}, \qquad (23)$$

$$\frac{\partial \overline{\phi}(y,q)}{\partial y}\bigg|_{y=0} = -\left(\frac{1}{q} + \overline{\phi}(0,q)\right), \overline{\phi}(y,q) \to 0; y \to \infty. \quad (24)$$

The solution of Eq. (23) with transformed conditions in Eq. (24) will be yielded as

$$\overline{\phi}(y,q) = \frac{\sqrt{q^{\gamma}}}{\sqrt{\mathrm{Pr}_{\mathrm{eff}}\left[(1-\gamma)q^{\gamma}+\gamma\right]q} - \sqrt{q^{\gamma}}} \frac{e^{-y\sqrt{\frac{\mathrm{Pr}_{\mathrm{eff}}\, q\left[(1-\gamma)q^{\gamma}+\gamma\right]}{q^{\gamma}}}}}{q}. \quad (25)$$

To obtain the Laplace transform inversion of Eq. (25), we utilized the Stehfest and Tzou numerical methods as in Table 1. In this subsection, we have found the solution for temperature distribution based on the AB fractional derivative by employing the Laplace method.

Concentration profile

Taking Laplace transform on Eqs. (12 and 22) and conforming conditions (14)$_3$–(16)$_3$, we get

$$\frac{\partial^2 \overline{\psi}(y,q)}{\partial y^2} - \mathrm{Sc}_{\mathrm{eff}}(q+k)\frac{\left[(1-\gamma)q^{\gamma}+\gamma\right]}{q^{\gamma}}\overline{\psi}(y,q) = 0, \quad (26)$$

$$\overline{\psi}(y,q) = \frac{1}{q}, \overline{\psi}(y,q) \to 0; y \to \infty. \quad (27)$$

By employing the above conditions of Eq. (27) and after simplification, Eq. (26) gives the concentration field

$$\overline{\psi}(y,q) = \frac{e^{-y\sqrt{\mathrm{Sc}_{\mathrm{eff}}(q+k)\frac{\left[(1-\gamma)q^{\gamma}+\gamma\right]}{q^{\gamma}}}}}{q}. \quad (28)$$

The Laplace inverse of Eq. (28) will be examined in Table 1 numerically. In this subsection, we have found the solution for the concentration profile based on the AB fractional derivative by employing the Laplace technique.

Velocity field

Taking the Laplace transform on Eq. (9) and corresponding conditions (14)$_1$–(16)$_1$, we get

$$\mathrm{Re}\frac{\partial^2 \overline{w}(y,q)}{\partial y^2} - q\overline{w}(y,q) - M\sin(\theta_1)\overline{w}(y,q) \quad (29)$$
$$= -\mathrm{GrCos}(\theta_2)\overline{\phi}(y,q) - \mathrm{Gm}\,\mathrm{Cos}(\theta_2)\overline{\psi}(y,q),$$

$$\overline{w}(0,q) - h\frac{\partial \overline{w}(y,q)}{\partial y}\bigg|_{y=0} = \frac{q}{q^2+\omega^2}, \overline{w}(y,q) \to 0; y \to \infty. \quad (30)$$

By using the conditions of Eq. (30) and temperature solution from Eq. (25) and the concentration value from Eq. (28), the solution of the momentum Eq. (29) is

$$\overline{w}(y,q) = \left(\begin{array}{c} \frac{q}{q^2+\omega^2} + \frac{\mathrm{Gr}\cos(\theta_2)}{q\mathrm{Re}}\frac{\sqrt{q^{\gamma}}}{\sqrt{q\mathrm{Pr}_{\mathrm{eff}}\left[(1-\gamma)q^{\gamma}+\gamma\right]}}\frac{1+h\sqrt{\mathrm{Pr}_{\mathrm{eff}}\frac{q\left[(1-\gamma)q^{\gamma}+\gamma\right]}{q^{\gamma}}}}{\frac{-\sqrt{q^{\gamma}}\left[(1-\gamma)q^{\gamma}+\gamma\right]q\mathrm{Pr}_{\mathrm{eff}}}{q^{\gamma}} - \frac{q+M\sin(\theta_1)}{\mathrm{Re}}} \\ + \frac{\mathrm{Gm}\cos(\theta_2)}{\mathrm{Re}q}\frac{1+h\sqrt{\mathrm{Sc}_{\mathrm{eff}}(q+k)\frac{q\left[(1-\gamma)q^{\gamma}+\gamma\right]}{q^{\gamma}}}}{\mathrm{Sc}_{\mathrm{eff}}(k+q)\frac{\left[(1-\gamma)q^{\gamma}+\gamma\right]}{q^{\gamma}} - \frac{q+M\sin(\theta_1)}{\mathrm{Re}}} \end{array}\right)\frac{1}{1+h\sqrt{\frac{q+M\sin(\theta_1)}{\mathrm{Re}}}}e^{-y\sqrt{\frac{q+M\sin(\theta_1)}{\mathrm{Re}}}}$$

$$- \frac{\mathrm{Gr}\cos(\theta_2)}{\mathrm{Re}q}\frac{\sqrt{q^{\gamma}}}{\sqrt{q\mathrm{Pr}_{\mathrm{eff}}\left[(1-\gamma)q^{\gamma}+\gamma\right]} - \sqrt{q^{\gamma}}}\frac{e^{-y\sqrt{\mathrm{Pr}_{\mathrm{eff}}\frac{q\left[(1-\gamma)q^{\gamma}+\gamma\right]}{q^{\gamma}}}}}{\frac{\left[(1-\gamma)q^{\gamma}+\gamma\right]q\mathrm{Pr}_{\mathrm{eff}}}{q^{\gamma}} - \frac{q+M\sin(\theta_1)}{\mathrm{Re}}}$$

$$- \frac{\mathrm{Gm}\cos(\theta_2)}{\mathrm{Re}q}\frac{e^{-y\sqrt{\frac{\left[(1-\gamma)q^{\gamma}+\gamma\right]}{q^{\gamma}}\mathrm{Sc}_{\mathrm{eff}}(k+q)}}}{\mathrm{Sc}_{\mathrm{eff}}(k+q)\frac{\left[(1-\gamma)q^{\gamma}+\gamma\right]}{q^{\gamma}} - \frac{q+M\sin(\theta_1)}{\mathrm{Re}}}. \quad (31)$$

Table 1 Numerical results of concentration, temperature, and momentum profile through Stehfest as well as Tzou's technique

y	ψ by Stehfest	ψ by Tzou	ϕ by Stehfest	ϕ by Tzou	W by Stehfest	W by Tzou
0.1	0.87814	0.85593	1.3181	1.3182	2.3908	2.3895
0.3	0.67719	0.67821	0.93671	0.93696	2.796	2.7971
0.5	0.52204	0.52209	0.6567	0.6569	2.8729	2.874
0.7	0.40213	0.40215	0.45394	0.45409	2.759	2.76
0.9	0.30936	0.30938	0.30922	0.30933	2.5444	2.5452
1.1	0.23756	0.23758	0.20747	0.20756	2.2863	2.2871
1.3	0.18201	0.18202	0.13705	0.13712	2.0196	2.0204
1.5	0.13905	0.13905	0.089097	0.08915	1.7642	1.7649
1.7	0.10587	0.10588	0.056981	0.05702	1.5301	1.5307
1.9	0.080299	0.080299	0.035837	0.035864	1.3215	1.322

The Laplace inversion of above Eq. (31) will be examined in Table 1 numerically.

Gradients

The present research also addresses the three essential variables of engineering curiosity: the Nusselt number, the Sherwood number, and shear stress. The aforementioned gradients can be expressed mathematically as:

Nusselt number

$$\text{Nu} = -\left.\frac{\partial \phi(y,t)}{\partial y}\right|_{y=0} = -\mathcal{L}^{-1}\left\{\frac{\partial \overline{\phi}(0,q)}{\partial y}\right\}.$$

Sherwood number

$$\text{Sh} = -\left.\frac{\partial \psi(y,t)}{\partial y}\right|_{y=0} = -\mathcal{L}^{-1}\left\{\frac{\partial \overline{\psi}(0,q)}{\partial y}\right\}.$$

Skin friction

$$C_f = -\left.\frac{\partial w(y,t)}{\partial y}\right|_{y=0} = -\mathcal{L}^{-1}\left\{\frac{\partial \overline{w}(0,q)}{\partial y}\right\}.$$

For the Laplace inversion, numerous investigators have used diverse numerical inverse approaches. So, here, we will also utilize the Stehfest technique [47] to investigate the solution of thermal, concentration, and momentum profiles numerically. Gaver-Stehfest method [47] mathematically may be simulated as

$$w(y,t) = \frac{\ln(2)}{t} \sum_{m=1}^{P} u_m \overline{w}\left(y, m\frac{\ln(2)}{t}\right) \tag{32}$$

where P is a positive integer, and

$$u_m = (-1)^{m+\frac{P}{2}} \sum_{i=\left[\frac{q+1}{2}\right]}^{\min\left(q,\frac{P}{2}\right)} \frac{i^{\frac{P}{2}}(2i)!}{\left(\frac{P}{2}-i\right)!i!(i-1)!(q-i)!(2i-q)!}$$

Nevertheless, we have also hired another approximation to find the solution of concentration, energy, and momentum profile, Tzou's method for the validity and comparison of our attained numerical consequences by the Stehfest method. Tzou's technique [48] can be demarcated as

$$w(y,t) = \frac{e^{4.7}}{t}\left[\frac{1}{2}\overline{w}\left(i, \frac{4.7}{t}\right) + \text{Re}\left\{\sum_{j=1}^{P}(-1)^k\overline{w}\left(i, \frac{4.7+k\pi l}{t}\right)\right\}\right] \tag{33}$$

where l is an imaginary unit and Re(.) is the real part and $P > 1$ is the natural number.

In this subsection, we have found the solution for velocity distribution based on the AB fractional derivative by employing the Laplace technique. Furthermore, we also found the three essential variables of engineering curiosity i.e. Nusselt number, Sherwood number, and Skin friction. In the end, we included a comparison for the validation of the codes for the Gaver–Stehfest method [47] and Tzou's technique [48].

Results with discussion

The physical characteristics of the MHD free convective fractionalized viscous fluid model based on the AB derivative having a non-singular and non-local kernel to investigate
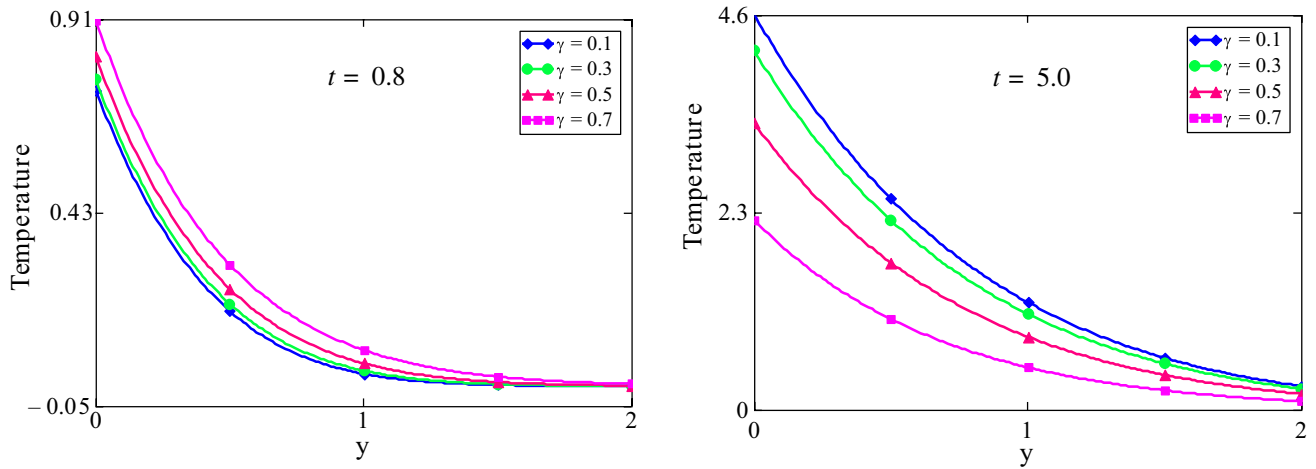
Fig. 2 Simulation for temperature with a variation of γ when Pr = 2.2, Re = 0.5
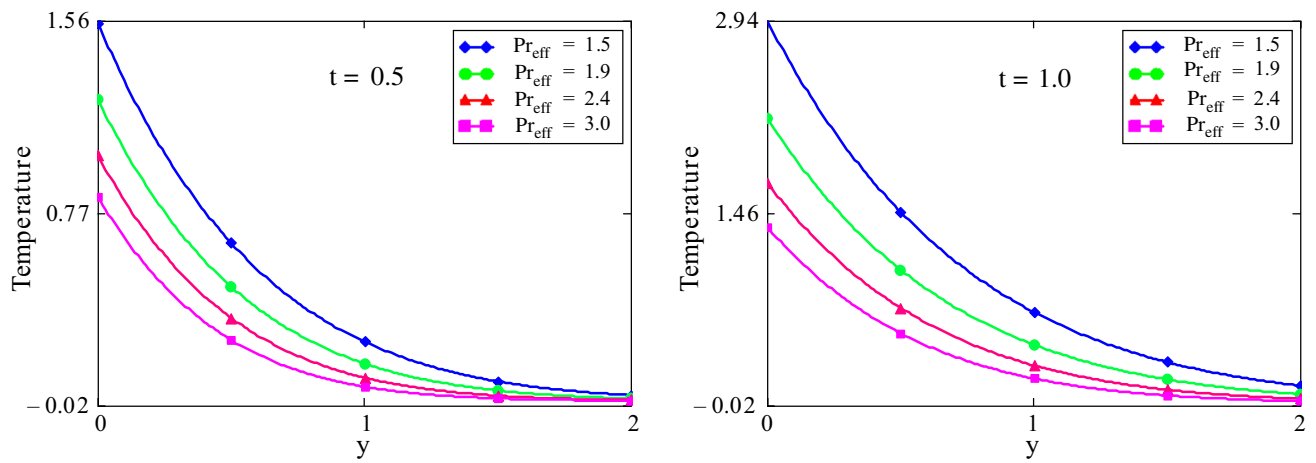
Fig. 3 Simulation for temperature with the variation of Pr_{eff} when $\gamma = 0.5$
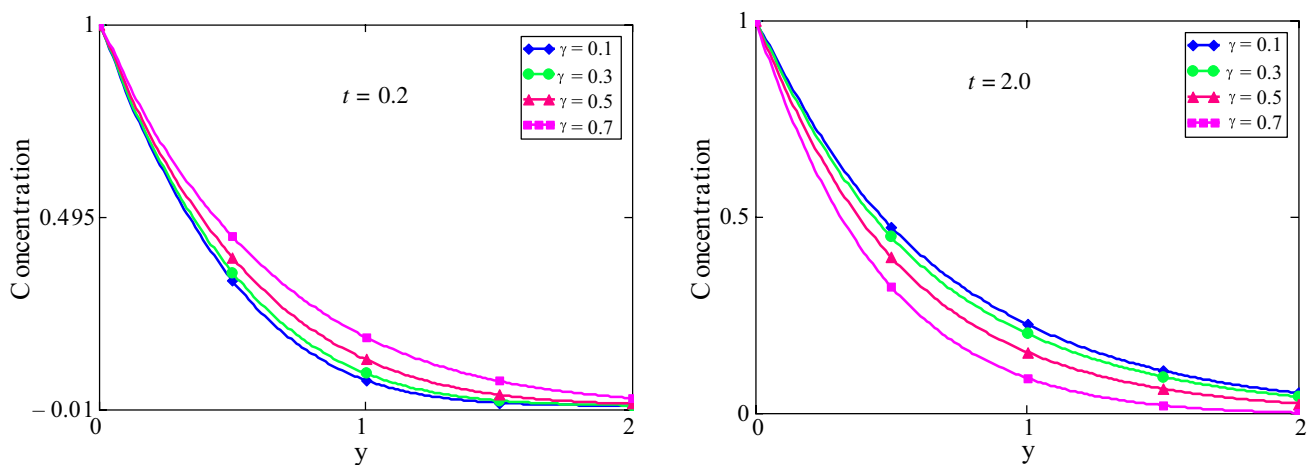
Fig. 4 Simulation for concentration with the variation of γ when Sc = 0.22, K = Re = 0.5
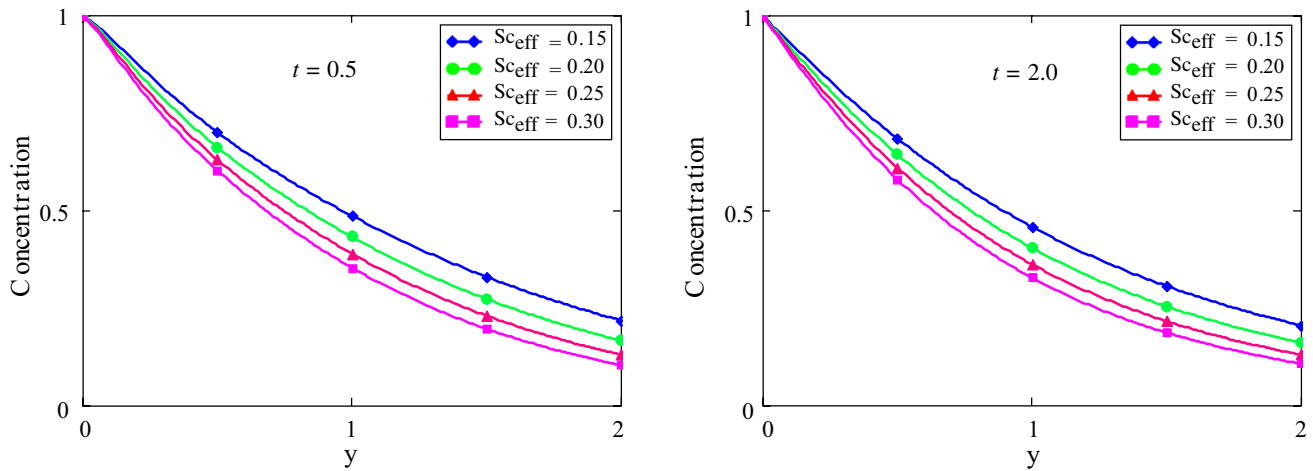
Fig. 5 Simulation for concentration with the variation of Sc_{eff} when $\gamma = 0.5$, $K = 2$

the slip and Newtonian heating effect are studied. Furthermore, the joint effect of thermal, mass, and velocity transfer has been taken into our study by demonstrating graphs for diverse estimations of the time. The graphical analysis illustrates the impacts of different fractional and flow parameters i.e. γ, Gr, Gm, Pr_{eff}, Re, Sc_{eff}, M, and the angle of magnetic fields' inclination (θ_1) for the physical understanding of the found results for energy, momentum, and concentration profiles on the MHD fluid flowing over an inclined oscillating plate in Figs. 2–14 through Mathcad15

Figure 2 is organized to examine the impacts of γ on the temperature distribution. By increasing the estimation of γ, the heat shows increasing behaviour for a small time and the fractional parameter shows the opposite behaviour for the temperature at a large time. This specifies the significance of

the AB fractional operator (a non-singular and non-local kernel) that assures to illustration of the extensive generalized memory and hereditary characteristics. Figure 3 is planned to display the consequence of effective Prandtl number Pr_{eff} on the energy profile. The effective Prandtl number is the ratio of Prandtl number Pr and Reynolds number Re. The Pr is a dimensionless measure that clarifies the connection between the energy as well as velocity boundary layer thickness. The higher the values of Pr_{eff} results from the higher values of Pr. In heat transfer problems, the thinner energy boundary layer in comparison with the velocity boundary layer is due to greater Pr, which outcomes in a lessening in the energy profile at small and large times. Hence, Pr may be applied to increase the rate of cooling.
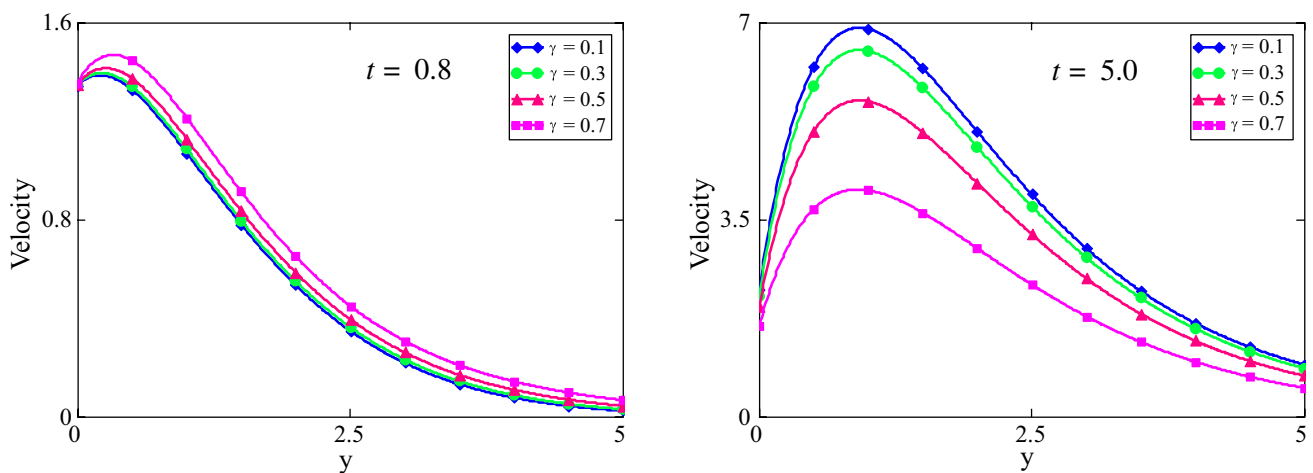

Fig. 6 Simulation for velocity with the variation of γ when $Pr = 2.2$, $Sc = 0.22$, $Re = 1.0$, $Gr = 8$, $Gm = 4.5$, $K = 0.5$, $M = 1$, $\theta_1 = \phi = \frac{\pi}{4}$, $h = 0.2$
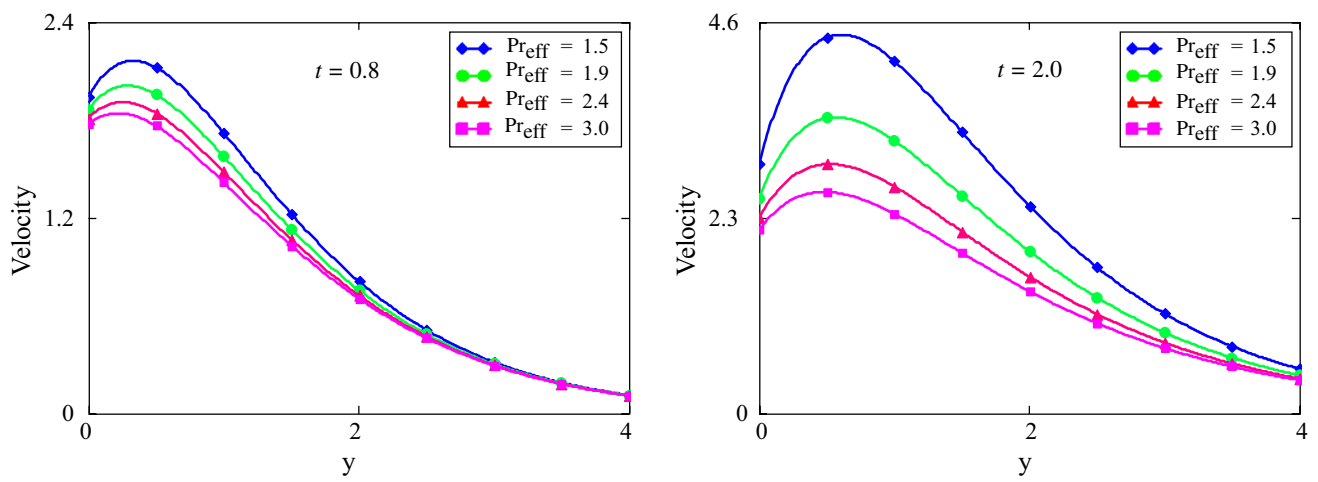
Fig. 7 Simulation for the velocity at changing $\mathrm{Pr}_{\mathrm{eff}}$ when $\gamma = 0.5, \mathrm{Sc} = 0.5, \mathrm{Re} = 1.5, \mathrm{Gr} = 5, \mathrm{Gm} = 6.5, K = 1, M = 0.5, \theta_1 = \phi = \frac{\pi}{4}, h = 0.2$
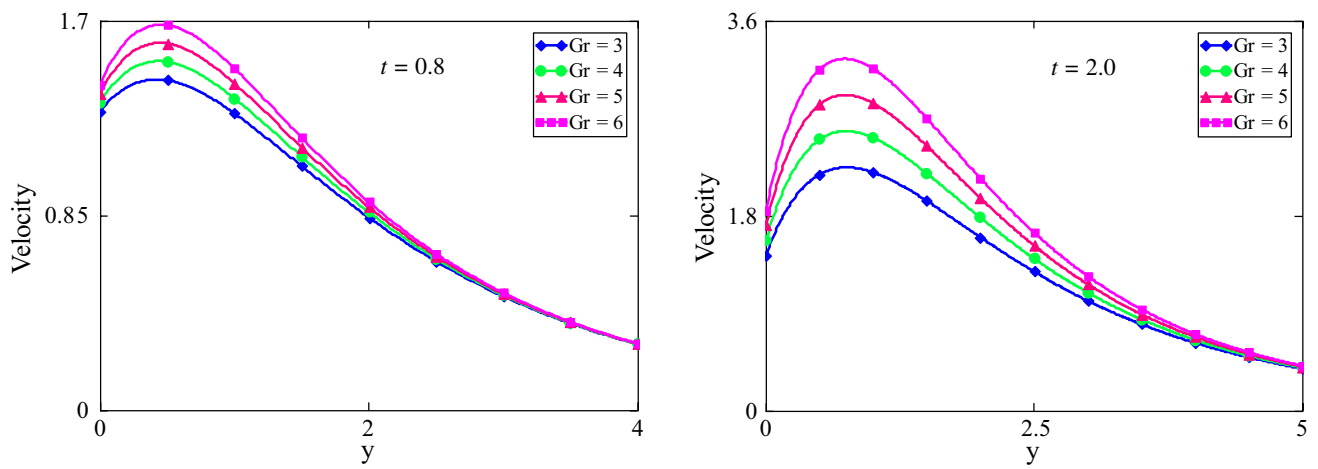
Fig. 8 Simulation for velocity with variation of Gr when $\gamma = 0.5, \mathrm{Sc} = 0.22, \mathrm{Pr} = 2.2, \mathrm{Re} = 1.5, \mathrm{Gm} = 4.5, K = 2.5, M = 1, \theta_1 = \phi = \frac{\pi}{4}, h = 0.2$
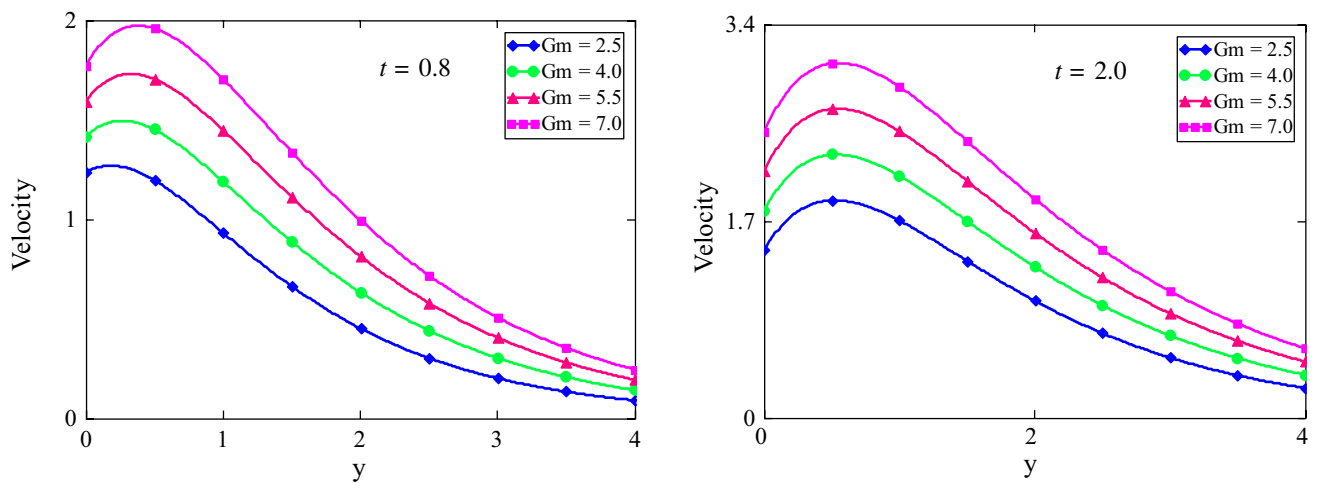
Fig. 9 Simulation of velocity for variation of Gm when $\gamma = 0.5, \mathrm{Sc} = 0.22, \mathrm{Pr} = 2.2, \mathrm{Re} = 1.5, K = 2.5, M = 1, \theta_1 = \phi = \frac{\pi}{4}, h = 0.2, \mathrm{Gr} = 5$
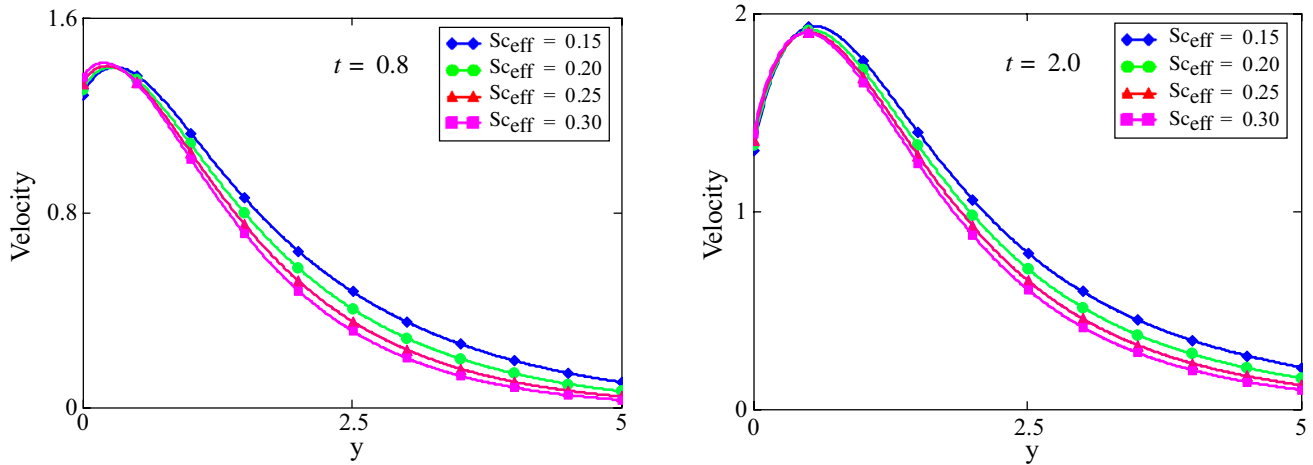
Fig. 10 Simulation of velocity for variation of Sc_{eff} when $\gamma = 0.5, Gr = 5, Pr = 2.5, Re = 1.5, Gm = 6.5, K = 1, M = 0.5, \theta_1 = \phi = \frac{\pi}{4}, h = 0.2$
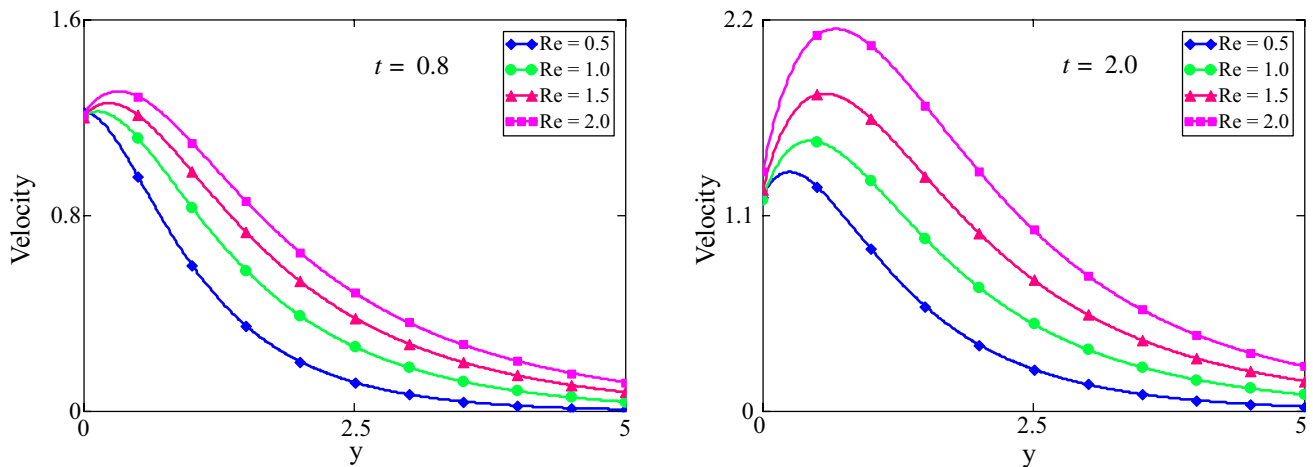

Fig. 11 Simulation of velocity with a variation of Re when $\gamma = 0.5, Sc = 0.5, Gr = 5, Gm = 6.5, K = 1, M = 0.5, \theta_1 = \phi = \frac{\pi}{4}, h = 0.2, Pr = 2.2$

Figure 4 displays the influence of γ on the concentration. A gradual increase (at a small time) and decreasing behaviour (at a large time) can be observed as γ rises. This is also due to the significance of the AB fractional operator (a non-singular and non-local kernel) that assures to illustration of the extensive generalized memory and hereditary characteristics. Figure 5 exposes the result of Sc_{eff} on the concentration. The effective Schmidt number Sc_{eff} resulted from the dimensionless numbers i.e. Schmidt Sc and Reynolds Re. It is found that at small and larger times values-enhancing Sc_{eff} which makes concentration levels fall. This may be enlightened by the detail that Sc is the ratio among viscous forces as well as mass diffusivity, so an intensification in Sc raises the viscous forces, and therefore, the concentration declines.

Figure 6 exposes the effects of γ on the momentum profile. This can be detected that at a smaller time growing, the estimation of γ leads to enhancing and declining (at a larger time) the velocity profile. This is also due to the implication of the AB fractional operator (a non-singular and non-local kernel) that assures to illustration of the extensive generalized memory and hereditary characteristics. Also, velocity decreases away from the plate as well as asymptotically rises in y-direction, which is also denoting the considered conditions. The effects of Pr_{eff} on the rate of velocity are studied in Fig. 7. The velocity decreases by growing Pr_{eff}. An increase in Pr_{eff} leads from increasing Pr which decreases the energy boundary layer thickness. The Pr denotes the ratio of momentum diffusivity to energy diffusivity. The increasing
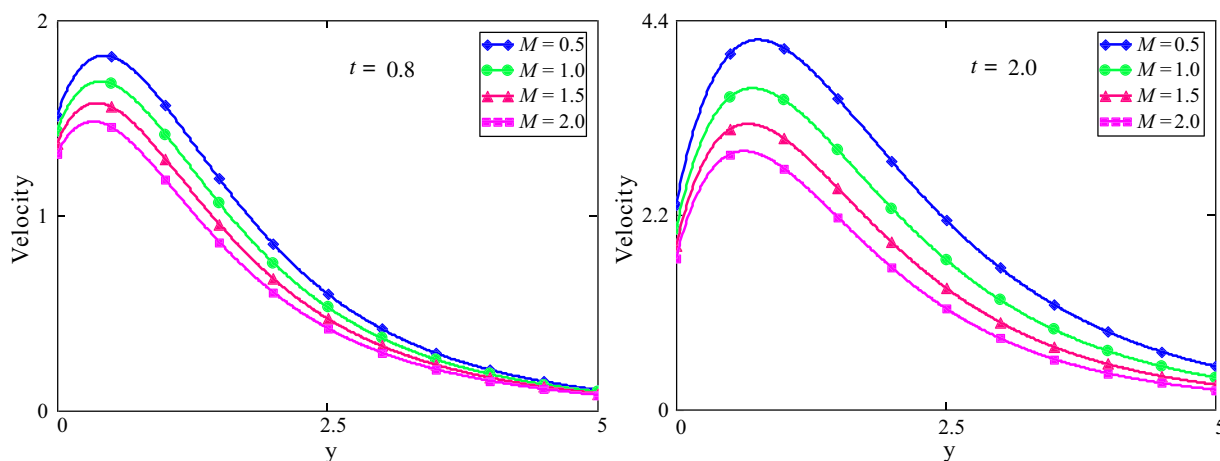
Fig. 12 Simulation for velocity with the variation of M when $\gamma = 0.5, \mathrm{Gr} = 5, \mathrm{Pr} = 2.2, \mathrm{Re} = 1.5, \mathrm{Sc} = 0.22, \mathrm{Gm} = 6.5, K = 1, \theta_1 = \phi = \frac{\pi}{4}, h = 0.2$
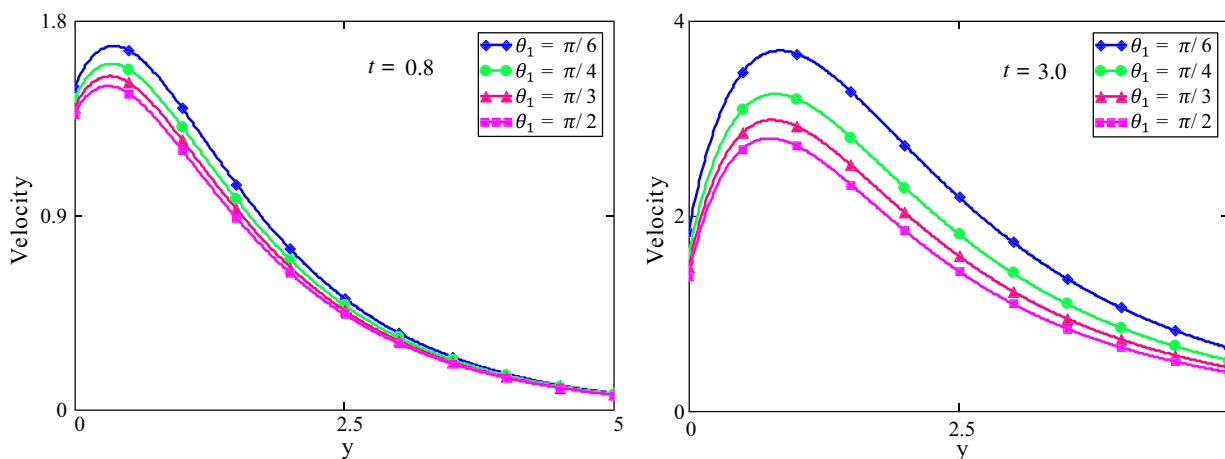
Fig. 13 Simulation for the velocity at changed values of θ_1 when $\gamma = 0.5, \mathrm{Gr} = 5, \mathrm{Pr} = 2.2, \mathrm{Re} = 1.5, \mathrm{Sc} = 0.22, \mathrm{Gm} = 6.5, K = 1, \phi = \frac{\pi}{4}, h = 0.2, M = 1$

value of Pr raises the thickening of the momentum boundary layer compared to thermal boundary layers. That's why velocity declines for growing estimation of $\mathrm{Pr}_{\mathrm{eff}}$ for different times.

The Grashof number is significant for the reason that it depicts the ratio of resistive forces arising from fluid viscosity to buoyant forces coming from spatial variation as well as fluid density. Figures 8 and 9 illustrate velocity profiles for various values of Gr and Gm. Increased values of these parameters produce forces of buoyancy, leading to higher induced flows. As Gr and Gm are increased, the fluid's velocity improves as a result.

Figure 10 determines the result of $\mathrm{Sc}_{\mathrm{eff}}$ on the velocity. It is exposed that growing the estimation of $\mathrm{Sc}_{\mathrm{eff}}$ declines the

velocity. This is clarified by the element that Sc is the ratio of viscous forces as well as mass diffusivity, so growth in Sc grows the viscous forces and therefore declines the velocity. Figure 11 exhibited that the reduction in velocity profile resulted from enhancing the value of Re. Re is the ratio of inertial forces and viscous forces (friction forces of two fluid elements moving to each other). An increasing value of Re decreases the viscous forces, so velocity is enhanced.

Figure 12 and 13 reveal the impact of magnetic parameter M and angle θ_1 of magnetic effect on the velocity profile. M is a dimensionless number that is rendered with Lorentz force that counters fluid velocity. The advanced value of M leads to a higher Lorentz force, which opposes movement.
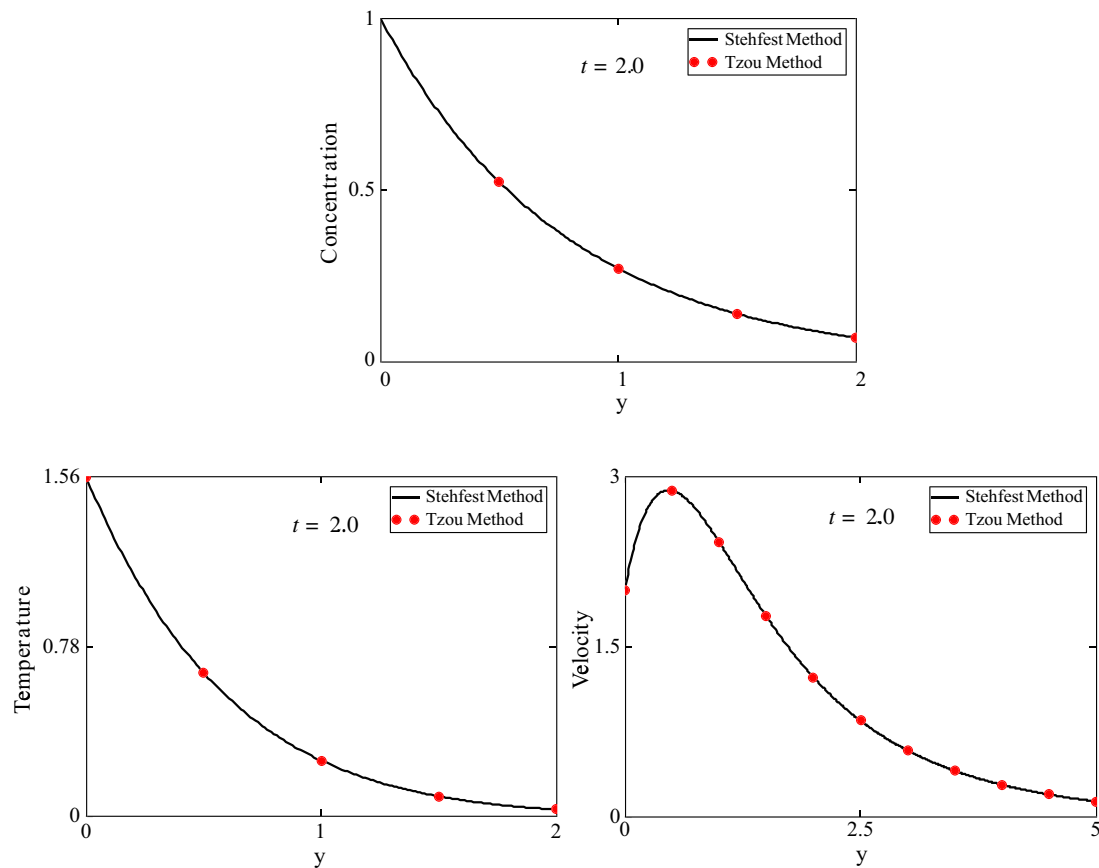
Fig. 14 Comparison of the velocity, concentration, and temperature profiles with different numerical algorithms

Table 2 Numerical results of Nusselt number and Sherwood number, as well as skin friction

α	Nu at $t = 0.2$	Nu at $t = 2.0$	Sh at $t = 0.2$	Sh at $t = 2.0$	C_f at $t = 0.2$	C_f at $t = 2.0$
0.1	1.2975	2.6103	1.9595	1.0598	1.7246	0.21429
0.2	1.3063	2.6057	1.9536	1.089	1.7134	0.22738
0.3	1.3206	2.5972	1.9362	1.1385	1.6962	0.2482
0.4	1.3415	2.5821	1.9041	1.2087	1.674	0.27589
0.5	1.3707	2.5559	1.8558	1.2997	1.6476	0.30982
0.6	1.4119	2.5102	1.7909	1.4115	1.6171	0.35002
0.7	1.4723	2.4317	1.7106	1.5437	1.5817	0.3976
0.8	1.5679	2.3027	1.6191	1.6951	1.5384	0.45405
0.9	1.7361	2.1172	1.5306	1.8634	1.4801	0.5148

So, velocity is reduced with growing M. Likewise, the angle of a magnetic field θ_1 stronger the stimulus of M which is transferred by the Lorentz force. For $\theta_1 = \pi/2$ (normal magnetic field), the effect of the Lorentz force is maximum, so lowers the velocity. Figure 14 is plotted for comparing two diverse numerical methods, Stehfest as well as Tzou for thermal, concentration, and velocity curves. The obtained results from diverse profile curves have overlapped with each other, signifying this research work's validity. (Table 2)

Conclusions

In this attempt, the flow of unsteady, viscous, MHD flow over an infinite inclined oscillating plate along with an AB fractional derivative (having a non-singular and non-local kernel) with the Mittag-Leffler function is invoked for developing the fractional model to study the memory effects. The effects of Newtonian heating as well as slip conditions are also taken to be under consideration. The

Laplace approach is employed to obtain the solution for governing equations of energy and concentration, as well as velocity. The main key points are enumerated below:

- The profiles of concentration and temperature, as well as velocity increased for a small time by enhancing γ and asymptotically declined at a large time.
- The effective Prandtl and Schmidt numbers decrease the thermal and concentration, as well as velocity levels of the fluid.
- Velocity profiles are boosted by enhancing the value of Gr and Gm because of the growth in the buoyancy effect.
- The velocity profile shows a trend of increasing and declining by improving the estimations of the Reynolds number and magnetic parameter, respectively.
- The solution curves of temperature, momentum, and concentration fields with numerical techniques i.e. Stehfest and Tzou coincided with each other which assures the validation of our achieved results.

Consequently, our claimed results offer significant insights into industrial and engineering systems. These findings guide the development of thermal transfer technologies, assisting in the optimization of processes for better efficiency in applications such as cooling mechanisms and power generation. The research advances heat transfer processes, increasing the overall efficiency of industrial systems.

Future recommendations

To extend the problem addressed in this paper, we propose the following ideas based on the analysis, geometries, methodologies, and expansions stated below:

- The Prabhakar and Caputo-Fabrizio fractional operators may be used to study the same problem in channel flow with a permeable medium.
- The same problem may also be explored using the fractional natural decomposition method (FNDM) and the Keller Box approach.
- A comparison investigation of this fractional model may also be performed by using the natural and Laplace transforms.

References

1. Shirvan KM, Mamourian M, Mirzakhanlari S, Rahimi AB, Ellahi R. Numerical study of surface radiation and combined natural convection heat transfer in a solar cavity receiver. Int J Numer Methods Heat Fluid Flow. 2017;105:811–25.
2. Alamri SZ, Khan AA, Azeez M, Ellahi R. Effects of mass transfer on MHD second grade fluid towards stretching cylinder: a novel perspective of Cattaneo-Christov heat flux model. Phys Lett A. 2019;383(2–3):276–81.
3. Shah NA, Elnaqeeb T, Wang S. Effects of Dufour and fractional derivative on unsteady natural convection flow over an infinite vertical plate with constant heat and mass fluxes. Comput Appl Math. 2018;37(4):4931–43.
4. Shah NA, Elnaqeeb T, Animasaun IL, Mahsud Y. Insight into the natural convection flow through a vertical cylinder using caputo time-fractional derivatives. Int J Appl Comput Math. 2018;4(3):1–18.
5. Zhang J, Raza A, Khan U, Ali Q, Zaib A, Weera W, Galal AM. Thermophysical study of Oldroyd-B hybrid nanofluid with sinusoidal conditions and permeability: a Prabhakar fractional approach. Fractal Fract. 2022;6(7):357.
6. Akram S, Athar M, Saeed K, Razia A, Muhammad T. Role of thermal radiation and double-diffusivity convection on peristaltic flow of induced magneto-Prandtl nanofluid with viscous dissipation and slip boundaries. J Therm Anal Calorim. 2023;149:761–76.
7. Sadia H, Mustafa M. Numerical exploration of slip effects on second-grade fluid motion over a porous revolving disk with heat and mass transfer. Heliyon. 2023;9(8):e18683.
8. Abidin MZ, Ullah N, Hussain A, Saadaoui S, Mohamed MMI, Deifalla A. Case study of entropy optimization with the flow of non-Newtonian nanofluid past converging conduit with slip mechanism: an application of geothermal engineering. Case Stud Therm Eng. 2023;52:103764.
9. Ali Q, Amir M, Raza A, Khan U, Eldin SM, Alotaibi AM, Abed AM. Thermal investigation into the Oldroyd-B hybrid nanofluid with the slip and Newtonian heating effect: Atangana-Baleanu fractional simulation. Front Mater. 2023;10:1114665.
10. Ali Q, Riaz S, Memon IQ, Chandio IA, Amir M, Sarris IE, Abro KA. Investigation of magnetized convection for second-grade nanofluids via Prabhakar differentiation. Nonlinear Eng. 2023;12(1):20220286.
11. Amir M, Ali Q, Raza A, Almusawa MY, Hamali W, Ali AH. Computational results of convective heat transfer for fractionalized Brinkman type tri-hybrid nanofluid with ramped temperature and non-local kernel. Ain Shams Eng J. 2024;15(3):102576.
12. Amir M, Ali Q, Abro KA, Raza A. Characterization nanoparticles via Newtonian heating for fractionalized hybrid nanofluid in a channel flow. J Nanofluids. 2023;12(4):987–95.

13. Vieru D, Fetecau C, Fetecau C, Nigar N. Magnetohydrodynamic natural convection flow with Newtonian heating and mass diffusion over an infinite plate that applies shear stress to a viscous fluid. Zeitschrift für Naturforschung A. 2014;69(12):714–24.

14. Das M, Mahato R, Nandkeolyar R. Newtonian heating effect on unsteady hydromagnetic Casson fluid flow past a flat plate with heat and mass transfer. Alex Eng J. 2015;54(4):871–9.

15. Ramzan M. Influence of Newtonian heating on three dimensional MHD flow of couple stress nanofluid with viscous dissipation and joule heating. PLoS ONE. 2015;10(4):e0124699.

16. Ramzan M, Farooq M, Alsaedi A, Hayat T. MHD three-dimensional flow of couple stress fluid with Newtonian heating. Eur Phys J Plus. 2013;128(5):1–15.

17. Hayat T, Hussain M, Alsaedi A, Shehzad SA, Chen GQ. Flow of power-law nanofluid over a stretching surface with Newtonian heating. J Appl Fluid Mech. 2014;8(2):273–80.

18. Ullah I, Shafie S, Khan I. Effects of slip condition and Newtonian heating on MHD flow of Casson fluid over a nonlinearly stretching sheet saturated in a porous medium. J King Saud Univ Sci. 2017;29(2):250–9.

19. Kamran M, Wiwatanapataphee B. Chemical reaction and Newtonian heating effects on steady convection flow of a micropolar fluid with second order slip at the boundary. Eur J Mech-B/Fluids. 2018;71:138–50.

20. Kamran M. Heat source/sink and Newtonian heating effects on convective micropolar fluid flow over a stretching/shrinking sheet with slip flow model. Int J Heat Technol. 2018;36(2):473–82.

21. Gangadhar K, Vijaya Kumar D, Venkata Subba Rao M, Kannan T, Sakthivel G. Effects of Newtonian heating on the boundary layer flow of non-Newtonian magnetohydrodynamic nanofluid over a stretched plate using spectral relaxation method. Int J Ambient Energy. 2022;43(1):1248–61.

22. Khan D, Khan A, Khan I, Ali F, Tlili I. Effects of relative magnetic field, chemical reaction, heat generation and Newtonian heating on convection flow of Casson fluid over a moving vertical plate embedded in a porous medium. Sci Rep. 2019;9(1):1–18.

23. Ahmad K, Wahid Z, Hanouf Z. Heat transfer analysis for Casson fluid flow over stretching sheet with Newtonian heating and viscous dissipation. J Phys: Conf Ser. 2019;1127(1):012028.

24. Caputo M. Linear models of dissipation whose Q is almost frequency independent—II. Geophys J Int. 1967;13(5):529–39.

25. Caputo M, Fabrizio M. A new definition of fractional derivative without singular kernel. Prog Fract Diff Appl. 2015;1(2):73–85.

26. Losada J, Nieto JJ. Properties of a new fractional derivative without singular kernel. Prog Fract Differ Appl. 2015;1(2):87–92.

27. Atangana A, Baleanu D (2016) New fractional derivatives with nonlocal and non-singular kernel: theory and application to heat transfer model. arXiv preprint arXiv:1602.03408

28. Lin Y, Raza A, Khan U, Nigar N, Elattar S, AlDerea AM, Khalifa HAEW. Prabhakar fractional simulation for thermal and solutal transport analysis of a Casson hybrid nanofluid flow over a channel with buoyancy effects. J Magn Magn Mater. 2023;586:171176.

29. El-Zahar ER, Al-Boqami GF, Al-Juaydi HS. Approximate analytical solutions for strongly coupled systems of singularly perturbed convection-diffusion problems. Mathematics. 2024;12(2):277.

30. Demir İ, Tunç T. New midpoint-type inequalities in the context of the proportional Caputo-hybrid operator. J Inequal Appl. 2024;2024(1):2.

31. Chu YM, Bani Hani EH, El-Zahar ER, Ebaid A, Shah NA. Combination of Shehu decomposition and variational iteration transform methods for solving fractional third order dispersive partial differential equations. Numer Methods Part Diff Equ. 2024;40(2):e22755.

32. Raza N, Raza A, Ullah MA, Gómez-Aguilar JF. Modeling and investigating the spread of COVID-19 dynamics with Atangana-Baleanu fractional derivative: a numerical prospective. Phys Scr. 2024;99:035255.

33. Majeed AH, Bilal S, Mahmood R, Malik MY. Heat transfer analysis of viscous fluid flow between two coaxially rotated disks embedded in permeable media by capitalizing non-fourier heat flux model. Phys A. 2020;540:123182.

34. Majeed AH, Mahmood R, Shahzad H, Pasha AA, Islam N, Rahman MM. Numerical simulation of thermal flows and entropy generation of magnetized hybrid nanomaterials filled in a hexagonal cavity. Case Stud Therm Eng. 2022;39:102293.

35. Majeed AH, Irshad S, Ali B, Hussein AK, Shah NA, Botmart T. Numerical investigations of nonlinear maxwell fluid flow in the presence of non-Fourier heat flux theory: Keller box-based simulations. AIMS Math. 2023;8(5):12559–75.

36. Majeed AH, Mahmood R, Liu D, Ali MR, Hendy AS, Zhao B, Sajjad H. Flow and heat transfer analysis over a pair of heated bluff bodies in a channel: characteristics of non-linear rheological models. Case Stud Therm Eng. 2024;53:103827.

37. Mehmood A, Mahmood R, Majeed AH, Awan FJ. Flow of the bingham-papanastasiou regularized material in a channel in the presence of obstacles: correlation between hydrodynamic forces and spacing of obstacles. Modell Simul Eng. 2021;2021:1–14.

38. Ahmad H, Mahmood R, Hafeez MB, Majeed AH, Askar S, Shahzad H. Thermal visualization of Ostwald-de Waele liquid in wavy trapezoidal cavity: effect of undulation and amplitude. Case Stud Therm Eng. 2022;29:101698.

39. Khan Y, Majeed AH, Rasheed MA, Alameer A, Shahzad H, Irshad S, Faraz N. Dual solutions for double diffusion and MHD flow analysis of micropolar nanofluids with slip boundary condition. Front Phys. 2022;10:956737.

40. Hussain Majeed A, Mahmood R, Hamadneh NN, Siddique I, Khan I, Alshammari N. Periodic flow of non-Newtonian fluid over a uniformly heated block with thermal plates: a hybrid mesh-based study. Front Phys. 2022;10:195.

41. Awan AU, Shah NA, Ahmed N, Ali Q, Riaz S. Analysis of free convection flow of viscous fluid with damped thermal and mass fluxes. Chin J Phys. 2019;60:98–106.

42. Tassaddiq A, Khan I, Nisar KS. Heat transfer analysis in sodium alginate based nanofluid using MoS_2 nanoparticles: Atangana-Baleanu fractional model. Chaos Solitons Fract. 2020;130:109445.

43. Ali Q, Riaz S, Awan AU, Abro KA. Thermal investigation for electrified convection flow of Newtonian fluid subjected to damped thermal flux on a permeable medium. Phys Scr. 2020;95(11):115003.

44. Awan AU, Ali Q, Riaz S, Shah NA, Chung JD. A thermal optimization throughan innovative mechanism of free convection flow of Jeffrey fluid using non-local kernel. Case Stud Therm Eng. 2021;24:100851.

45. Ali Q, Riaz S, Awan AU, Abro KA. A mathematical model for thermography on viscous fluid based on damped thermal flux. Zeitschrift für Naturforschung A. 2021;76(3):285–94.

46. Awan AU, Riaz S, Abro KA, Siddiqa A, Ali Q. The role of relaxation and retardation phenomenon of Oldroyd-B fluid flow through Stehfest's and Tzou's algorithms. Nonlinear Eng. 2022;11(1):35–46.

47. Stehfest H. Algorithm 368: numerical inversion of laplace transforms [D5]. Commun ACM. 1970;13(1):47–9.

48. Tzou DY. Macro-to microscale heat transfer: the lagging behavior. Wiley; 2014.